MEMS Graphene Strain Sensor

Clinton Young, Liang Dong

Department of Electrical and Computer Engineering, Iowa State University, Ames, IA 50011

Keywords: Graphene sensor, rosette design, graphene patterning, graphene transfer

ABSTRACT

In this paper, certain properties, such as the piezo-resistivity, of graphene will be explored to show how they can be utilized to make a stress sensing device. Our original fabrication process of patterning graphene and the transfer process of graphene onto a flexible substrate will be discussed. The development of a stretchable and flexible graphene based sensor will also be detailed. Many graphene sensors that have been developed are uni-directional. In other words, they can only measure the strain applied on the sensor in a principle direction which has limited real-world applications. This issue was solved in this paper by arranging the graphene sensors in a rosette pattern which enabled for multi-directional strain detection. The strain sensor was further improved by stacking the graphene sensors in a rosette pattern; which was possible by leveraging the advantages of soft lithography and bonding processes and the flexibility of graphene. Our final device was a stacked rosette graphene strain sensor that was able to measure strain in multiple directions and magnitudes simultaneously.

Highlights:

- We demonstrate a successful method for patterning graphene using lithography.
- We developed a successful method of transferring graphene onto a flexible PDMS substrate
- We demonstrate successful fabrication of a stack multi-layer graphene rosette strain senor

Keywords: Graphene sensor, rosette design, graphene patterning, graphene transfer

1. Introduction

Graphene is a material that has been generating interest in the microelectromechanical systems (MEMS) field due to its thinness, high carrier mobility [Chen, Nat. Nano tech., 3, 206 (2008)](4), high Young's modulus [C. Lee, Science 321, 385 (2008)](5), and numerous other properties [K. S. Novoselov, et al. Nature 11458, 2012] (3). Graphene is a single layer of Carbon atoms arranged in a hexagonal structure [A. K. Geim, Science 324, 2009](2), [K. S, Novoselov, Nautre 490, 2012] (3) and these attributes contribute to the exceptional electronic and mechanical properties of the material [C. Lee Science 321] (5), [Loh, The chemistry of graphene, J. Mat. Chem 20, 2010] (6).

The possible applications for graphene are being extensively researched [K. Novoselov, Roadmap, Nature] (3). The potential applications are numerous from graphene replacing silicon to graphene hybrid materials. However there are very few investigations in the MEMS field for using graphene as the strain sensing material in a sensor. It has been reported that graphene has a piezo-resistance response [Lee, Nano Lett. 2010] (7) and that it exhibits high sensitivity to stress [Fu X-W, Strain dependent resistance in CVD graphene, Appl Phys Lett., 2011] (8). Additionally, experiments have shown that graphene has excellent stretch ability and repeatability of stretching [Kim, K. S., et al. nature 07719, 2009] (9). These properties have made graphene a good candidate for stress and strain sensing applications.

In this paper, a Graphene-based MEMS pressure and strain sensor fabricated and patterned using a standard lithography process will be first presented as background information. The graphene strain sensor was transferred onto a thin, flexible plastic substrate after patterning. In addition a relatively simple method of patterning graphene using a standard lithography process and the method of transferring the graphene onto a flexible substrate of PDMS will be

discussed. Also, the process to manufacture a multi-directional strain sensor that eliminates the limitations of a single strain gauge will be presented. The multi-directional strain sensor is manufactured by aligning 3 single strain gauges in Rosette manner to allow for measuring strain in multiple directions and magnitudes. Lastly, the consistency and repeatability of these strain sensors that are produced will be demonstrated.

2. Experimental details

The processing diagram of our graphene fabrication method is show in Figure 1.

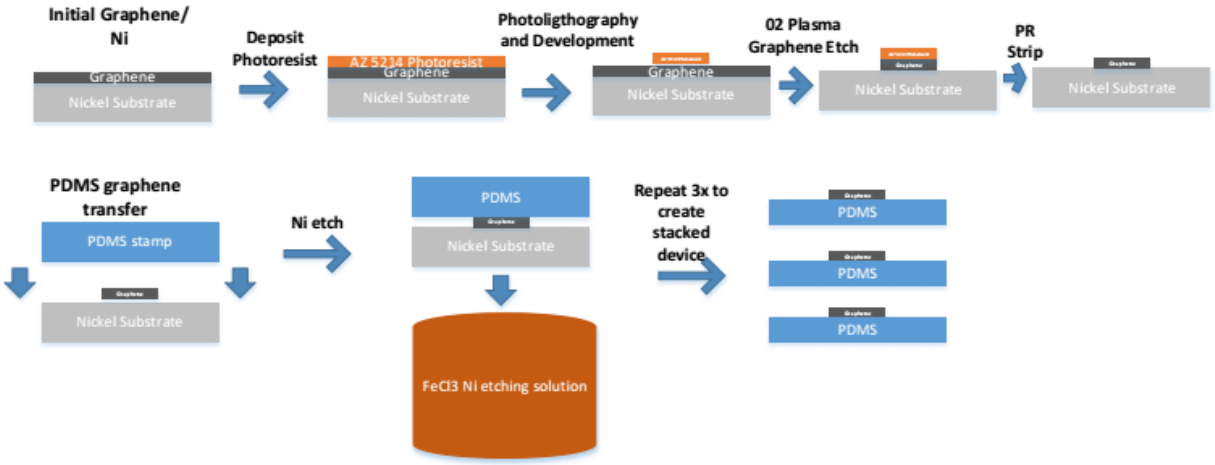

Figure 1: Fabrication Process Overview.

The photolithography process begins by depositing a photoresist to form and protect the desired pattern on the graphene. The initial CVD graphene on nickel was spin coated with the photoresist AZ5214 at a rate of 500 rpm for 25 seconds, this spin speed ensured a layer of ~10 um of photoresist that will be used to protect the graphene during the etching process. A thick layer of photoresist was needed because graphene is a tough material to etch due to the strength of its carbon bonds, therefore etching was a long process and the photoresist needed to resist through the etching process to protect our pattern graphene. After the thick layer of photoresist was spin coated onto the graphene a pre-bake process followed; the sample was baked at 90 degree Celsius for 15 minutes to drive off excess photoresist solvent and to harden the photoresist.

The next step the photolithography process is ultraviolet (UV) light exposure of the photoresist. The mask also determines the desired pattern that will be etched into the graphene.

The mask is aligned with the graphene and placed in the UV exposure area. The photoresist covered graphene is then exposed to intense UV light for 90 seconds at 2mW/cm^2, this causes a chemical change in the exposed areas of photoresist so that is becomes soluble to be removed by the developer solution. The graphene is then submerged into photoresist developer, to remove the exposed areas of photoresist, and developed for 2 minutes and 30 seconds. The development time is determined by the thickness of the photoresist and due to the thick layer of photoresist, a long developer time is needed to ensure complete removal of photoresist for etching process. Post-bake or hard-baking process of 120 degrees Celsius for 10 minutes reinforced the photoresist to make it more resistant to the 02 plasma etching process used for etching graphene.

For the fabrication procedure, the graphene etching is done with an o_2 oxygen plasma etcher Diener electric. The graphene is placed in the plasma etcher, the air is vacuumed from the chamber, and then oxygen is flowed at a low pressure into the chamber and excited into plasma through dielectric breakdown. Process settings for the plasma etching were: 100% power, 8sccm (standard cubic centimeter per minute) oxygen flow rate, oxygen pressure of 8Pa. The graphene etching process took 1 hour. Following the etching process, the photoresist had to be removed from the graphene and the graphene was also removed from the silicon wafer base that it was attached to during this process. The use of acetone stripped away the photoresist on the graphene pattern and the resist holding the graphene to the silicon base. After a rinse to clean the surface of the graphene, it is now ready for the transfer process.

Figure 1: Post Graphene Etch Graphene/Ni. Ready for transfer process

The unique aspect of our patterning process is that with a change of the mask it is possible to create different patterns, sizes, and shapes on the graphene. Research focused on graphene patterning, the patterns are typically micron to millimeter sized feature sizes, and it is easier to pattern on a bigger scale for large-scale graphene work. This makes our patterning process adaptable to many research applications. This method makes vast improvements to current methods of patterning graphene. It is completely adaptable to desired patterns, great resolution of feature sizes, and incorporates a common process semiconductor process.

2.2 Graphene Transfer

A transfer method that combined both wet and dry methods was developed, and this allowed for the utilization of the advantages of both methods. The use of a PDMS stamp was used as a substrate and a nickel etching solution of ferric chloric acid was used to etch away the initial nickel substrate in a wet transfer.

Figure 3: Graphene/Ni in metal etching solution.

Figure 4: Graphene successfully transferred onto PDMS.

A PDMS stamp was made by mixing PDMS and curing agent with a ratio of 15:1, as mentioned above this ratio was determined to have the best characteristics needed for graphene transfer. The liquid mixture was then put into a vacuum chamber for 60mins to remove any air

bubbles trapped in the PDMS from the mixing process. By removing any air bubbles it ensured that the fabricated PDMS stamp would be smooth for best surface adhesion to the graphene. Next the PDMS was poured on a glass slide to create a flat smooth surface and then it was cured on a hot plate for 1 hour at 75 degrees Celsius to create the PDMS stamp. At this temperature and time, it ensured that the PDMS stamp was cured enough to work with as a stamp yet maintained enough tackiness to adhere to the graphene [Yoo, Takei; Nanotechnology 24, 2013] (56). If the PDMS was cured at too high of a temperature, this decreased the cross-linking of PDMS to graphene and the flexibility of the stamp is decreased. If the PDMS was cured at too low of a temperature, the PDMS would under-cure and formed a gel instead of a stamp. These effects also occurred at too high of a time or too low of a time. The flat smoothness of the PDMS stamp is of crucial importance to ensure good surface to surface bonding between the graphene and the PDMS. The PDMS stamp was fabricated on a glass slide to make sure the stamp was a smooth flat surface.

Once the PDMS stamp was created, it needed to be attached to the patterned graphene. Make sure the graphene is flat and on a solid flat surface, slowly attach PDMS stamp smoothly onto the graphene. Apply pressure on the PDMS stamp to ensure good adhesion to graphene and to remove any air trapped between the two. Once the PDMS stamp was well attached to the patterned graphene it was then placed into the metal etching solution.

The nickel etching solution was a ferric chloride solution that was prepared with 27 grams of ferric chloride and 300 ml of DI water or (~0.1 g/ml). The PDMS/graphene/Ni slab was placed into the etching solution for 24 hours until the Ni was etched completely away Figure 3 and 4.

An aqueous iron (III) chloride (FeCl3) solution (1 M) was used as an oxidizing etchant to remove the nickel substrate. The net ionic equation of the etching reaction is:

$$2 * Fe^{3+}(aq) + Ni(s) \rightarrow 2 * Fe^{2+}(aq) + Ni^{2+}(aq)$$

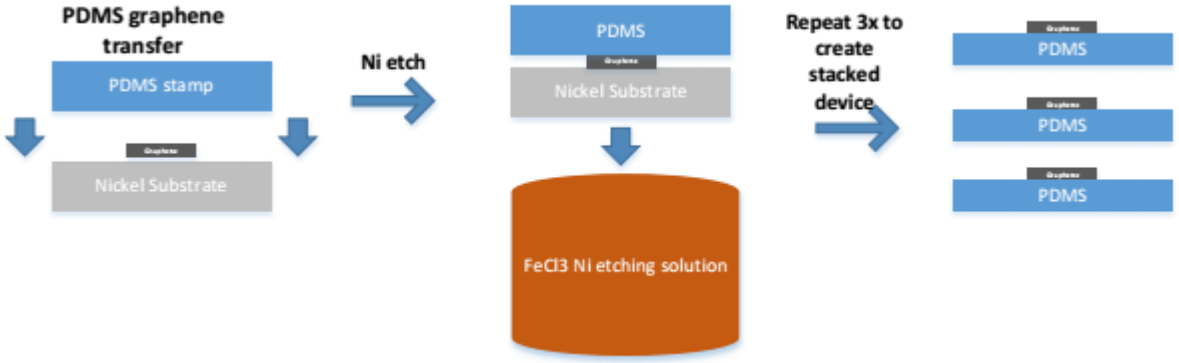

2.2.3 Raman spectroscopy tests

Raman spectroscopy is an important part of graphene research. It can be used to determine the number of layers of graphene present, the quality and type of graphene, and the effects that strain, doping, stress, electric and magnetic fields have on graphene [57]. Raman spectroscopy is the ideal tool that provides fast, high resolution, non-destructive characterization of graphene [58]. The use of Raman was used in our research to confirm the successful transfer of graphene and to obtain an estimation of how many layers of graphene were transferred.

There are three main peaks of phonon scattering in graphene that detail important properties. At a frequency around 1550 cm^{-1} there is a peak called the G peak which is observable in all carbon materials, only the optical phonon with zero momentum is present at this specific frequency. A 2D peak with frequency around 2700 cm^{-1} is indicative of second order Raman scattering. This 2D peak is the resonant scattering in which the incident photon energy coincides with the real energy band. The fewer layers of graphene that are present, the sharper the 2D peak will be at 2700cm^{-1}. The sharpness of the 2D peak for our graphene indicates there

are at most 10 layers of graphene present. If defects are present in the graphene, this may lead to the "D" peak.

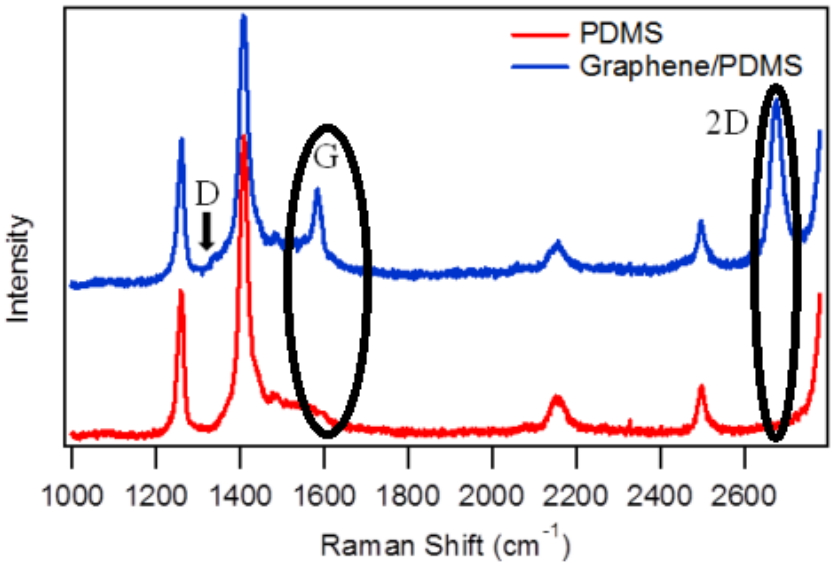

Figure 6: comparison of the peaks, providing evidence of successful graphene transfer

2.3 Flexible Graphene Sensors

2.4.1 Single graphene sensor

A strain gauge is a device that measures strain. It works by having a flexible backing that supports a metallic foil pattern. This gauge is attached to an object and as that object is deformed, the foil also undergoes deformation which caused the electrical resistance to change. Instead of a metal foil, the patterned graphene is the resistance changing element in the sensor. A single graphene sensor consisted of a pattern graphene resistor attached to a PDMS substrate. As strain is applied with a tensile bench to the graphene, the resistance can be measured with a multi-meter. Results show that as strain is applied, the resistance shows a linear trend of increase with the strain applied. However a single resistor is limited in its real-world applications.

To improve the robustness and stability of our graphene contacts during strain testing, liquid metal was injected to reinforce the contact areas. This prevented the graphene contacts from deteriorating when strain was applied during testing. The liquid metal also had the added benefit of enabling our device to maintain flexibility and made measurements of the different layers of the device easier.

2.4.2 Stacked rosette strain sensor

In the field of strain sensing, the rosette pattern is commonly used because it allows for multi-directional strain sensing. Rosettes are designed for experimental stress and strain analysis. A strain gauge rosette is an arrangement of two or more closely positioned gauges. In common cases where the principal directions of strain are unknown, all it takes is three independent strain measurements (all of different directions) to determine the principal strains or vice versa. However where most devices have a planar rosette pattern, due to the flexibility of graphene, it is possible to stack our devices to form the rosette pattern and this is advantageous over current planar rosette sensors. A stacked rosette minimizes sensor size yet is still able to

measure multiple directions and magnitudes of stress to a very precise point. In traditional MEMS sensor fabrication with silicon, a stacked device is unfeasible due to the rigidness of the material. Graphene on the other hand is as flexible as the flexible substrate is it transferred onto which allows for a stackable strain sensing device.

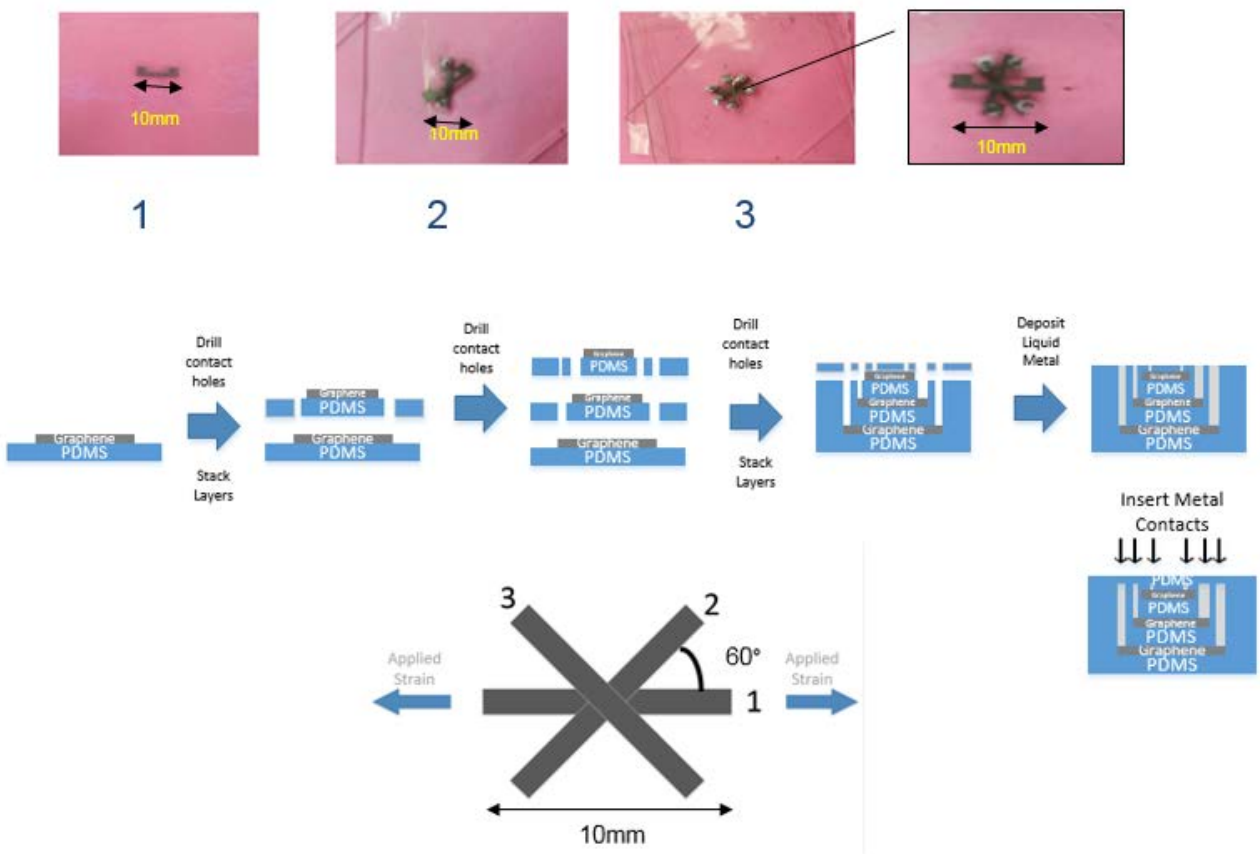

Figure 7: Final Design: Stacked Rosette Graphene Sensor.

Chapter 3: Device Performance and Results

3.1 Piezoresistive effect

To test the theory that graphene will change resistance when strain applied and it is a consistent and repeatable method for measuring resistance changes, our device was put on a strain stage that enabled us to apply controlled strain. Also required was to test whether this fabrication and transfer process produces a graphene pattern that will perform as expected. First to check the graphene pattern for completeness of patterning, transfer and connectivity, strain was applied to the graphene using a tensile stage and resistance change was measured using a multimeter. As can be seen in Figure 8, there is a linear correlation between the applied strain and change in resistance in the graphene. Deviations from this linear pattern occur when the graphene in the sensor is stretched past a certain point in which the graphene starts to break and tear.

The piezoresistive properties of graphene were tested by applying strain to a single graphene resistor. The van der Waals force between PDMS and graphene provide a strong adhesion and therefore the strain experienced by the PDMS is also experienced by the graphene. Figure 9 shows the measuring system setup to measure the piezoresistive properties of the graphene strain sensor. To measure the piezoresistivity, the PDMS with graphene sensor is stretched along a uniaxial direction at small increments 0.1mm (~0.01%). During the stretching, a multimeter was applied to the graphene strain sensor to measure the change in electrical resistance. In a neutral, no strain, position the distance between the two fixed ends was 10mm (0%) mm and at max strain the ends was measured at 11mm (10%). Throughout the test, the electrical resistance was continuously measured as a function of applied strain. As shown in Figure 8, as the strain applied increased, so did the resistance in a *linearly* fashion. It was discovered that if the graphene was stretched too much, cracks would form in the graphene

throwing off the electrical resistance. The graphene sensor does show good repeatability, the sensor underwent multiple trials of stretching and un-stretching and the electrical resistance was continuously measured. Figure 10 shows that the sensor showed good consistency in measuring the relationship of applied strain to electrical resistance and through that the relationship of applied strain and current. Typical electrical resistance of a commercial semiconductor strain gauge is 1kOhms.

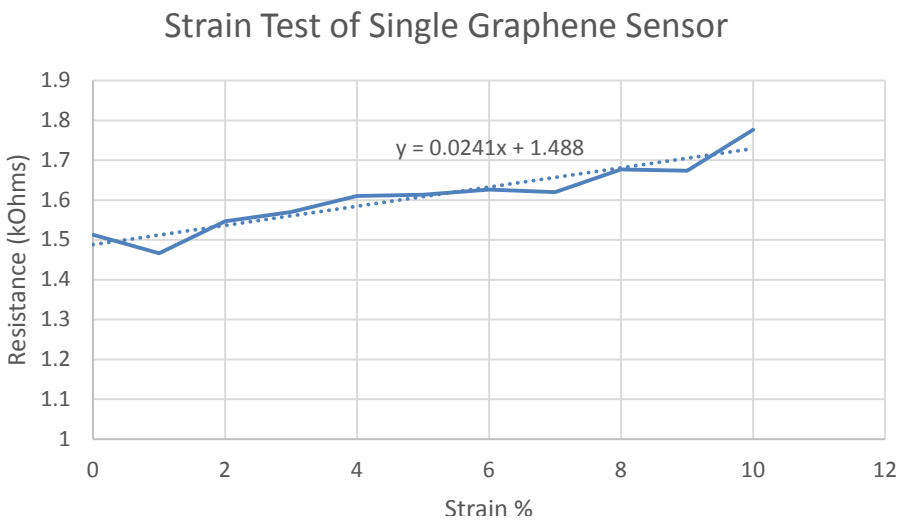

Figure 8: Strain Test of a Single Graphene-based Sensor.

5.2 Rosette design for multi-directionality

A single graphene based strain sensor is only capable of detecting strain or deformation in a singular direction. This limits the usefulness of the sensor in real-life applications. For characterization of complicated multi-directional deformations on a surface, it is necessary to measure strain in three dimensions, *eX, eY, eΘ*. To accomplish this, three of the same strain sensors are arranged to form a rosette, each sensor oriented at 120 degrees from each other forming an equilateral triangle formation. The placement of three equally spaced strain sensors, each with a fixed 60 degree angle from each other, is called a planar 60-delta rosette gauge

system Figure 22. The strain sensors in the rosette arrangement are named x, y, and z and their corresponding strain values *εx*, *εy*, and *εz*. By using the measured magnitudes of strain and the directions of the gauges, it is then possible to determine the full strain on the surface of the sensor location. The Mohr's circle, better known as the "strain transformation method", can graphically illustrate the surface state of strain Figure 22 (noting that the angles in Mohr's circle are double the physical angles on the test surface). The strain at any angle Θ from the major principal axis can be expressed as:

$$Strain = (eX + eY)/2 + (eX - eY)/2 * cos(2\theta) \quad \text{Eq. 3}$$

The strain on each rosette gauge can be represented in terms of principal strain on x and y axis with corresponding rotation angles Θ, Θ +60 degrees, and Θ +120 degrees. Using the following strain transformation equations it is possible to determine the directionality of the strain applied.

$$\varepsilon x = \frac{eX+eY}{2} + \frac{eX-eY}{2} * cos(2\theta) \quad \text{Eq. 4}$$

$$\varepsilon y = \frac{eX+eY}{2} + \frac{eX-eY}{2} * cos2(\theta + 60°) \quad \text{Eq. 5}$$

$$\varepsilon z = \frac{eX+eY}{2} + \frac{eX-eY}{2} * cos2(\theta + 120°) \quad \text{Eq. 6}$$

We can measure the strain values of *εx*, *εy*, and *εz*, and with those values it is possible to calculate the principal strain values x and y, and their orientation θ with the following equations.

$$eX,Y = \frac{\varepsilon x+\varepsilon y+\varepsilon z}{3} +/- \frac{\sqrt{2}}{3} * \sqrt{((\varepsilon x - \varepsilon y)^2 + (\varepsilon y - \varepsilon z)^2 + (\varepsilon z - \varepsilon x)^2)} \quad \text{Eq. 7}$$

$$\theta = \left(\frac{1}{2}\right) \tan^{-1} \left(\frac{\sqrt{3}*(\varepsilon y-\varepsilon z)}{2\varepsilon x-\varepsilon y-\varepsilon z}\right) \quad \text{Eq. 8}$$

[64]

The "+/-" in Eq. 4 is used to calculate the maximum and minimum principle strain, respectively, in Mohr's circle.

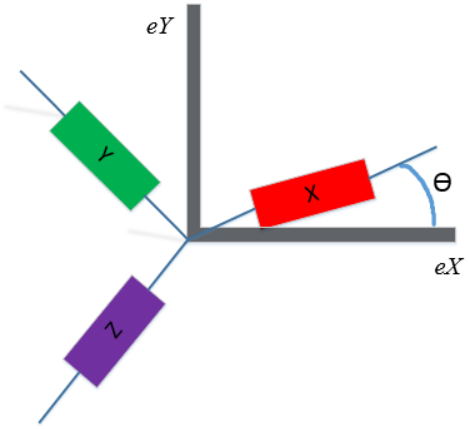

Figure 9: Direction of principal strain in a Rosette pattern.

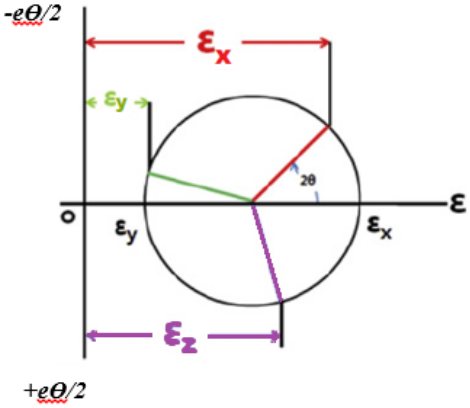

Figure 10: Mohr's circle diagram for strain analysis. Rosette axis superimposed on Mohr's circle for strain.

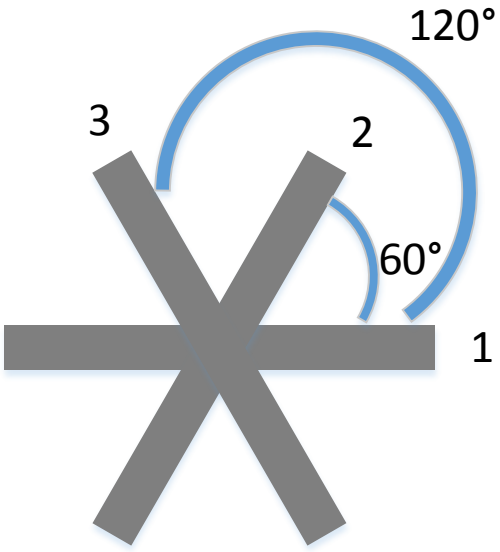

Figure 11: Delta rosette. Angle Θ from the major principal strain direction.

5.3 Stacked Multi-layered Device

Additionally, the rosette-type strain sensor was made up of 3 stacked devices instead of planar devices arranged in a rosette shape. The major disadvantage to a planar rosette is the larger surface area covered. Whereas a stacked rosette will occupy the least amount of area and has the center of all the gauges lying over the same point on the surface. Therefore a stacked rosette has better accuracy on strain measurements. The strain sensing device combines the multi-directional measuring abilities of a rosette pattern and it also improves upon this design by stacking the devices for better size management and signal resolution.

The strain sensing characteristics of the rosette shaped stacked device under stretching was investigated by the same method as that of the single graphene strain device, however now the resistance change of the three strain sensors was measured. Figure 24 shows the measurement of the resistances as a function of the applied strain for all three strain gauges. The stretching was applied along the x-axis, such that the ‘x’ gauge and the other two gauges were positioned at the same distance and oriented at the same angles with respect to the ‘x’ gauge. It was measured that as the strain was increased to the sensors, the resistances measured also increased. The change in the normalized resistance from the ‘x’ gauge was smaller than that of the other two gauges. As previously discussed, with the values of the strain on the three strain sensors known, the principal strain and their orientation with respect to the rosette axis can be estimated. The robustness of the device was tested by performing the strain test several times. Figure 25 shows the measurements of the three strain sensors, and it shows the change in the resistance repeated in the repeated strain tests. This verified that the fabricated rosette graphene strain device has a very robust capability of sensing strain.

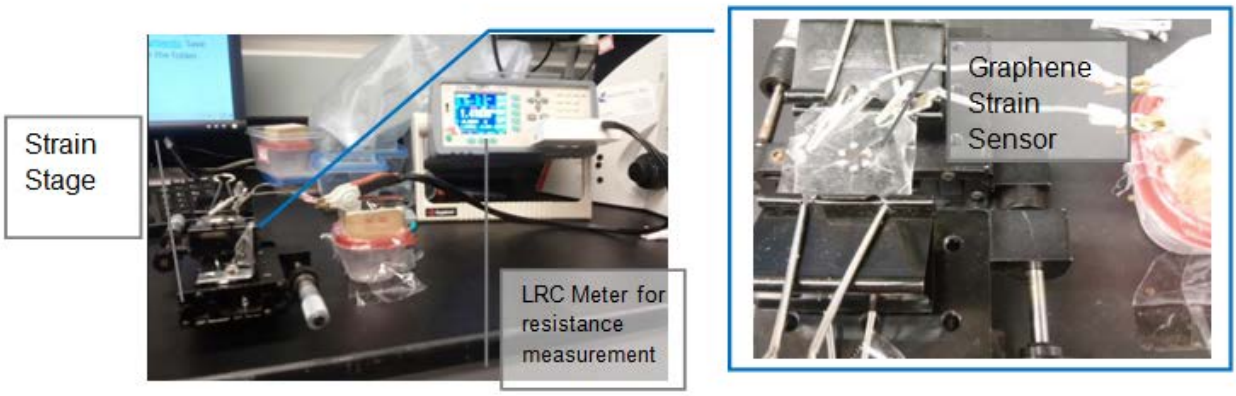

Figure 12: Strain Testing Setup.

The plots, shown in Figure 13, show the relationship between resistance and strain. As strain is increased, the resistances of the strain sensors linearly increase. Variations in the linear relation are due to breakage in the graphene and uneven stretching of the PDMS substrate. If there is a slight drop in resistance this is due to ripples in the graphene that are evening out as strain is applied. The stacked design of the sensor also contributes to the slight variations in resistance responses to the strain. But as the resistance plots shows, the sensors show similar and consistent responses to the same applied strain.

Each individual sensor was characterized, shown in Figure 13 and 14, a constant and consistent application of strain was applied to the device and the resistance for each sensor was measured. Strain values for sensors 1, 2, and 3 from this resistance-change data is calculated to 10%, 2.67%, and 2.67%, when the principal strain of about 10% is applied in the X-direction. As previously discussed, when the values of the three independent strains from the three sensors is known, the principal strains and their orientations with respect the rosette axis can be estimated. The principal strains *eX* and *eY* and their angle of orientation are calculated by inserting the three

stain values of the three sensors into Eq. 7 and 8 and are found to be 10%, 0.22%, and 0°, respectively. The calculated value of 10% for maximum principal strain (*eX)* matches the applied strain value, and this is indicative of good accuracy and sensing capability of the stacked graphene rosette strain sensor. The change in resistance characteristics repeated multiple times as the gradual increase and decrease of applied strain, and this verified that the fabricated stacked rosette graphene sensor showed a stable capability of sensing strain under repeated measurements.

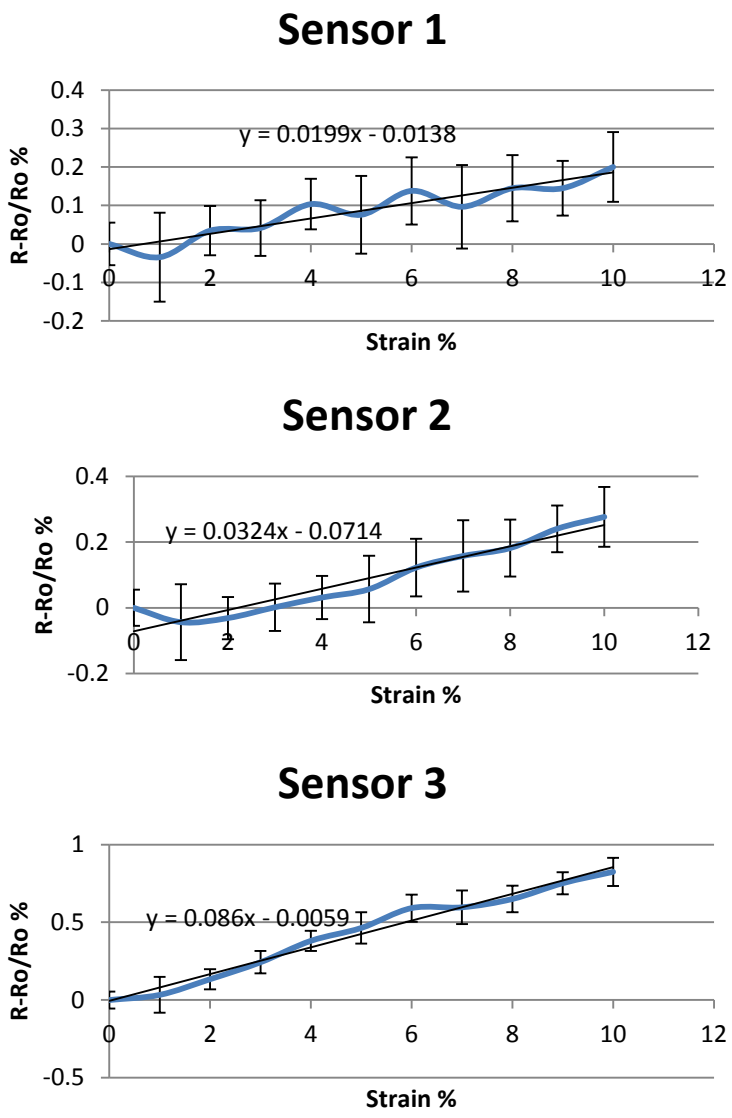

Figure 13: Multi-layer rosette strain plots.

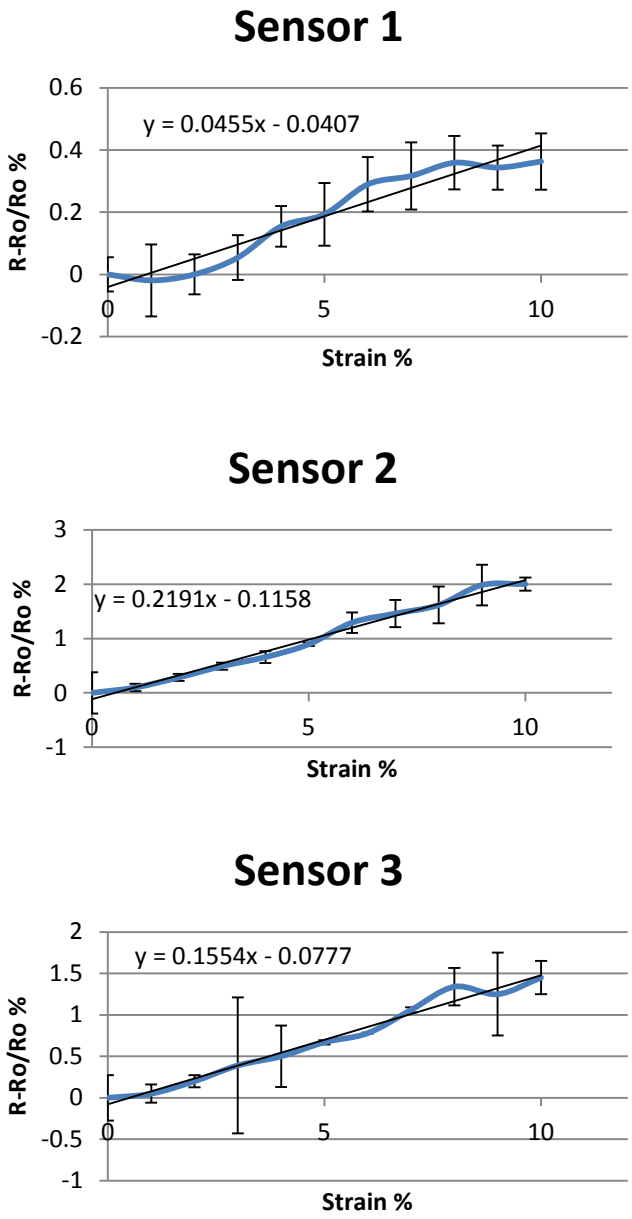

Figure 14: Multi-layer rosette strain plots measuring strain applied in Sensor 2 direction.

The angle of the direction of applied strain was also varied to test the ability of the sensor to measure the directionality of our graphene sensor. The device was rotated so that the direction of applied strain was in the same line as sensor 2 and the resistance was measured as strain was applied like before, shown in Figure 14. The strain values for sensors 1, 2, and 3 were measured as 2.67%, 10%, and 2.67% respectively. Using these strain values and Equations 7 and 8, the

principal strains *eX* and *eY* and their angle of orientation are calculated to be 10%, .22%, and -30°, respectively. The calculated value of 10% for maximum principal strain (*eX)* matches the applied strain value, however the angle was different from the expected value. Possible explanations for this is that during set-up the device was not rotated fully and so strain was not perfectly in-line with sensor 2, another explanation is that the calculations are correct and that our expected value is incorrect. This test does show that the strain sensor can detect variations of direction of applied strain and that it still accurately measures the principle strain values.

CHAPTER 4: SUMMARY

4.1 Conclusion

This paper presented a method of patterning and transferring graphene and demonstrated the successfulness of these methods by fabricating a stacked graphene rosette strain sensor. We have shown that the properties of graphene are useful for electronic and sensing applications. Both theoretical and experiment reports indicate that graphene is a viable candidate for flexible sensor applications. A graphene based piezoresistive strain sensor was fabricated by integrating graphene resistors on a flexible PDMS substrate. A reliable method of patterning graphene into a desired pattern and a method for transferring that graphene onto a flexible substrate was also developed. The use of graphene for high performance pressure sensor applications was demonstrated by the characteristics of the piezoresistive effect of graphene and the sensitivity of graphene to strain and pressure. Graphene's intrinsic flexibility, it allows for successful fabrication of a stacked device in a rosette pattern. Therefore a strain device in this configuration is able to detect magnitude and direction of principal strains in three dimensions and in a small area device.

4.2 Future work

The development of a reliable method of graphene patterning and transfer, this allows for stable isolation of graphene on a flexible substrate. These methods can be utilized in the fabrication of different types of graphene sensors and in the field of wearable electronics. Sensitivity of the graphene sensor can be further improved by integrating a full Wheatstone bridge into the graphene based sensing device. A Wheatstone bridge will increase the sensitivity of the graphene resistor allowing it to detect even smaller changes in strain.

References

1:Lundstrom, M. (2003). APPLIED PHYSICS: Enhanced: Moore's Law Forever? *Science,* 210-211.

2: Geim, A. Graphene: Status And Prospects. *Science,* 1530-1534.

3: Novoselov, K., Fal′ko, V., Colombo, L., Gellert, P. A roadmap for graphene. *Nature,* 192-200.

4: Chen, J., Jang, C., Xiao, S., Ishigami, M., & Fuhrer. Intrinsic and extrinsic performance limits of graphene devices on SiO2. *Nature Nanotechnology,* 206-209.

5: Lee, C., Wei, X., Kysar, J., & Hone. Measurement Of The Elastic Properties And Intrinsic Strength Of Monolayer Graphene. *Science,* 385-388.

6: Loh, K., Bao, Q., Ang, P., & Yang, J. The chemistry of graphene. *Journal of Materials Chemistry,* 2277-2277.

7: Lee, Y., Bae, S., Jang, H., Jang, S., Zhu, S., Sim, S. (2010). Wafer-Scale Synthesis and Transfer of Graphene Films. *Nano Letters,* 490-493.

8: Fu, X., Liao, Z., Zhou, J., Zhou, Y., Wu, H. Strain dependent resistance in chemical vapor deposition grown graphene. *Applied Physics Letters,* 213107-213107.

9. Kim, K., Zhao, Y., Jang, H., Lee, S., Kim, J., Kim, K., Hong, B. (2009). Large-scale pattern growth of graphene films for stretchable transparent electrodes. *Nature,* 706-710.

10: Novoselov, K. (n.d.). Electric Field Effect In Atomically Thin Carbon Films. *Science,* 666-669.

11: Mouras, S., Hamm, A., Djurado, D., Revue de Chimie Minerale 24(5), 572-582 (1987)

12: Dresselhaus, M., Dresselhaus, G., & Saito, R. (n.d.). Carbon fibers based on C60 and their symmetry. *Physical Review B,* 6234-6242.

13: A. H. Castro Neto, F. Guinea, N. M. R. Peres, K. S. Novoselov, and A. K. Geim. The electronic properties of graphene. Rev. Mod. Phys. 81, 109

14: J. N. Fuchs and M. O. Goerbig. Introduction to the Physical Properties of Graphene. Nano physics, 2008

15: Mermin, N., & Wagner, H. (n.d.). Absence of Ferromagnetism or Antiferromagnetism in One- or Two-Dimensional Isotropic Heisenberg Models. *Physical Review Letters,* 1133-1136.

16: Wee, A. (2012). Graphene: The Game Changer? *ACS Nano*, 5739-5741.

17: Geim, A., & Novoselov, K. (n.d.). The Rise of Graphene. *Nature Materials,* 183-191.

18: Novoselov, K. (n.d.). Electric Field Effect in Atomically Thin Carbon Films.*Science,* 666-669.

19: Kwon, S., Bae, W. and Kim. Korean Journal of Chemical Engineering, 21, 910-914

20: Saito, R.; Dresselhaus. Physical properties of carbon nanotubes; Impreial College: London, 1998

21: Zhou, S., Gweon, G., Graf, J., Fedorov, A., Spataru, C., Diehl, R., Lanzara, A. (2006). First direct observation of Dirac fermions in graphite. *Nature Physics*, 595-599.

22: Bolotin, K., Sikes, K., Jiang, Z., Klima, M., Fudenberg, G., Hone, J., Stormer, H. (n.d.). Ultrahigh electron mobility in suspended graphene.*Solid State Communications,* 351-355.

23: Murali, R., Yang, Y., Brenner, K., Beck, T., & Meindl, J. (n.d.). Breakdown current density of graphene nanoribbons. *Applied Physics Letters,* 243114-243114.

24: Meric, I., Han, M., Young, A., Ozyilmaz, B., Kim, P., & Shepard, K. (2008). Current saturation in zero-bandgap, top-gated graphene field-effect transistors. *Nature Nanotechnology*, 654-659.

25: Zhu, Y., Murali, S., Cai, W., Li, X., Suk, J., Potts, J., & Ruoff, R. (n.d.). Graphene-based Materials: Graphene and Graphene Oxide: Synthesis, Properties, and Applications (Adv. Mater. 35/2010). *Advanced Materials.*

26: Bae, S., Kim, H., Lee, Y., Xu, X., Park, J., Zheng, Y., Iijima, S. (2010). Roll-to-roll production of 30-inch graphene films for transparent electrodes. *Nature Nanotechnology*, 574-578.

27: Rafiee, M., Rafiee, J., Wang, Z., Song, H., Yu, Z., & Koratkar, N. (2009). Enhanced Mechanical Properties of Nanocomposites at Low Graphene Content. *ACS Nano,* 3884-3890.

28: Bogue, R. (n.d.). Nanosensors: A review of recent research. *Sensor Review*, 310-315.

29: Mohammed, A. Mechanical Strain Measurements Using Semiconductor Piezoresistive Material. Nano and Smart Systems, 2006

30: Sun, D., Aivazian, G., Jones, A., Ross, J., Yao, W., Cobden, D., & Xu, X. (2012). Ultrafast hot-carrier-dominated photocurrent in graphene. *Nature Nanotechnology,* 114-118.

31: Laukhina, E., Pfattner, R., Ferreras, L., Galli, S., Mas-Torrent, M., Masciocchi, N., Veciana, J. (2009). Ultrasensitive Piezoresistive All-Organic Flexible Thin Films. *Advanced Materials.*

32: Berger, C., Song, Z., Li, T., Li, X., Ogbazghi, A., Feng, R., Heer, W. (n.d.). Ultrathin Epitaxial Graphite: 2D Electron Gas Properties and a Route toward Graphene-based Nanoelectronics. *The Journal of Physical Chemistry B,* 19912-19916.

33: Hummers, W., & Offeman, R. (n.d.). Preparation of Graphitic Oxide. *Journal of the American Chemical Society,* 1339-1339.

34: Li, Y., Zhou, Z., Shen, P., & Chen, Z. (2009). Structural and Electronic Properties of Graphane Nanoribbons.*The Journal of Physical Chemistry C,* 15043-15045.

35: Li, X., Cai, W., Colombo, L., & Ruoff, R. (2009). Evolution of Graphene Growth on Ni and Cu by Carbon Isotope Labeling. *Nano Letters,* 4268-4272.

36: Apell, S. (n.d.). High optical absorption in graphene.

37: Multilayer Graphene on Nickel foil: 2"x2" (n.d.). Retrieved April 22, 2015, from https://graphene-supermarket.com/Multilayer-Graphene-on-Ni-foil-2-x2.html

38: Novoselov, K. (n.d.). Two-dimensional Atomic Crystals. *Proceedings of the National Academy of Sciences,*10451-10453.

39: Girit, C., Meyer, J., Erni, R., Rossell, M., Kisielowski, C., Yang, L., Zettl, A. (2009). Graphene at the Edge: Stability and Dynamics. *Science,* 1705-1708.

40: Ebbesen, T., & Hiura, H. (n.d.). Graphene in 3-dimensions: Towards graphite origami. *Advanced Materials,* 582-586.

41: Bai, J., Zhong, X., Jiang, S., Huang, Y., & Duan, X. (n.d.). Graphene Nanomesh. *Nature Nanotechnology,* 190-194.

42: Chen, Z., Lin, Y., Rooks, M., & Avouris, P. (n.d.). Graphene nano-ribbon electronics. *Physica E: Low-dimensional Systems and Nanostructures,* 228-232.

43: Tapasztó, L., Dobrik, G., Lambin, P., & Biró, L. (2008). Tailoring the atomic structure of graphene nanoribbons by scanning tunnelling microscope lithography. *Nature Nanotechnology,* 397-401.

44: Han, M., Özyilmaz, B., Zhang, Y., & Kim, P. (n.d.). Energy Band-Gap Engineering of Graphene Nanoribbons.*Physical Review Letters*.

45: Dimiev, A., Kosynkin, D., Sinitskii, A., Slesarev, A., Sun, Z., & Tour, J. (2011). Layer-by-Layer Removal of Graphene for Device Patterning. *Science,* 1168-1172.

46: Al-Mumen, H., Rao, F., Li, W., & Dong, L. (2014). Singular Sheet Etching of Graphene with Oxygen Plasma.*Nano-Micro Letters*.

47: Lee, J., Park, C., & Whitesides, G. (n.d.). Solvent Compatibility of Poly(dimethylsiloxane)-Based Microfluidic Devices. *Analytical Chemistry,* 6544-6554.

48: S. J. Clarkson and J. A. Semlyen, Siloxane Polymers, Prentice Hall, Englewood Cliffs, NJ, 1993.

49: Gates, B., Xu, Q., Stewart, M., Ryan, D., Willson, C., & Whitesides, G. (n.d.). New Approaches to Nanofabrication: Molding, Printing, and Other Techniques. *Chemical Reviews,* 1171-1196.

50: Kang, S. J. *et al*. Inking elastomeric stamps with micro-patterned, single layer graphene to create high-performance OFETs. *Adv. Mater.* **23**, 3531–3535(2011).

51: Reina, A., Jia, X., Ho, J., Nezich, D., Son, H., Bulovic, V., Kong, J. (n.d.). Large Area, Few-Layer Graphene Films on Arbitrary Substrates by Chemical Vapor Deposition. *Nano Letters,* 30-35.

52: Johnston, Mechanical characterization of bulk Sylgard 184. Journal of Micromechanics and MicroEng, 2014

53: Ko, P., Takahashi, H., Koide, S., Sakai, H., Thu, T., Okada, H., & Sandhu, A. (2013). Simple method to transfer graphene from metallic catalytic substrates to flexible surfaces without chemical etching. *Journal of Physics: Conference Series,* 012002-012002.

54: Kim, C., Woo, J., Choi, J., Park, J., & Han, C. (n.d.). Direct transfer of graphene without the removal of a metal substrate using a liquid polymer. *Scripta Materialia,* 535-537

55: Chang-Soo Han, Direct Transfer of Graphene.

56: Yoo, K., Takei, Y., Kim, S., Chiashi, S., Maruyama, S., Matsumoto, K., & Shimoyama, I. (2013). Direct physical exfoliation of few-layer graphene from graphite grown on a nickel foil using polydimethylsiloxane with tunable elasticity and adhesion. *Nanotechnology,* 205302-205302.

57: Ferrari, A., Meyer, J., Scardaci, V., Casiraghi, C., Lazzeri, M., Mauri, F., Geim, A. (n.d.). Raman Spectrum of Graphene and Graphene Layers. *Physical Review Letters*.

58: Ni, Z., Wang, Y., Yu, T., & Shen, Z. (n.d.). Raman spectroscopy and imaging of graphene. *Nano Research,* 273-291.

59: Raman, C., & Krishnan, K. (1928). A Theory of the Optical and Electrical Properties of Liquids. *Proceedings of the Royal Society A: Mathematical, Physical and Engineering Sciences,* 589-599.

60: Venkataraman, G., & Ramdas, A. (n.d.). Journey into Light: Life and Science of C. V. Raman. *Physics Today,* 61-61

61: Peplow, M. (2013). Graphene: The quest for supercarbon. *Nature,* 327-329.

62: Khoshnoud, F., & Silva, C. (n.d.). Recent advances in MEMS sensor technology-mechanical applications. *IEEE Instrumentation & Measurement Magazine,* 14-24.

63: Bae, S., Lee, Y., Sharma, B., Lee, H., Kim, J., & Ahn, J. (n.d.). Graphene-based transparent strain sensor. *Carbon,* 236-242.

64: Vishay. Strain Gage Rosettes: Selection, Application and Data Reduction. http://www.vishaypg.com/docs/11065/tn-515.pdf